Design of Amorphous Silicon Photonic Crystal-based M-Z Modulator Operating at 1.55 μm

Sandro Rao[1], Maurizio Casalino[2], Giuseppe Coppola[2], Rifat Kisacik[3], Tolga Tekin[3] and Francesco G. Della Corte[1,2]

[1]*Università degli Studi "Mediterranea", Dipartimento di Ingegneria dell'Informazione, delle Infrastrutture e dell'Energia Sostenibile (DIIES), Via Graziella Feo di Vito, 89122, Reggio Calabria, Italy*

[2]*Institute for Microelectronics and Microsystems – Consiglio Nazionale delle Ricerche (IMM-CNR) Via Castellino, 111, 80132, Napoli, Italy*

[3]*Fraunhofer Institute for Reliability and Microintegration (IZM), System Integration and Interconnection Technologies, Gustav-Meyer-Allee 25, 13355, Berlin, Germany*

Keywords: Photonic Crystal, Electro-optic Modulator, Amorphous Silicon.

Abstract: The design of an amorphous silicon-based Mach–Zehnder electro-optic modulator including two guiding p-i-n structures integrated inside a two-dimensional (2-D) photonic crystal (PhC) working at 1.55 μm, is reported. Electrically induced free carrier dispersion effect in this photonic material with a very cost-effective technology, is investigated for modulation. Our numerical analysis, performed by a time-domain (FDTD)-based software, proves that the voltage-length product can be remarkably reduced by taking advantage of both the strong PhC confinement and the wide refractive index tunability of amorphous silicon.

1 INTRODUCTION

The incorporation of optical phase modulators into slow wave structures can offer advantages in terms of both reduced device length and low power consumption. This is due to the interaction enhancement between the refractive index variation mechanism and the propagating optical mode (Vlasov et al., 2005). The latter property is particularly interesting to develop highly-compact photonic devices based on the engineered change of the signal optical phase within the waveguide. Among the different devices, the Mach–Zehnder interferometer (MZI) acquires a fundamental importance because it can be used as a basic building block of more complex photonic devices such as optical filters, wavelength multiplexers, intensity modulators, switches and optical gates (Reed et al., 2010).

The technology of low-absorption hydrogenated amorphous silicon (a-Si:H) has been recently demonstrated to be a promising low cost and CMOS compatible platform for combining electronic integrated circuits with active optical functions, that could make feasible the three-dimensional (3D) integration of complex photonic-electronic integrated circuits (PEICs) (Della Corte and Rao,2013).

Recently, an a-Si:H based MZI electro-optic (EO) modulator has been experimentally demonstrated (Rao et al., 2012). In such device we exploited the free carrier depletion approach, within a reverse biased waveguide integrated p-i-n diode, in order to reduce the transient characteristics with respect to the field-induced accumulation-type devices (Zelikson et al., 1992; Della Corte et al., 2008; Rao et al., 2010; Rao et al., 2013). Electrons and holes are in fact quickly swept from the "active" layer where light propagates when a bias is applied across the device.

Such configuration allowed to reach for the first time a modulation bandwidth larger than 150 Mbps in as-deposited a-Si:H-based devices (Rao et al., 2014).

The Factor of Merit (FoM) $V_\pi \times L$ has been measured to be about 40 V×cm, although in an optimized setup with a reduced thickness of the waveguide core, i.e. down to 400 nm-thick, the modulating pulse amplitude, V_π, is expected to decrease by a factor of ~10 (Della Corte et al., 2011).

On the other hand, in order to get a modulation efficiency enhancement, for a given fixed geometry, the relative overlap between the optical field distribution within the waveguide core and the

Rao, S., Casalino, M., Coppola, G., Kisacik, R., Tekin, T. and Corte, F.
Design of Amorphous Silicon Photonic Crystal-based M-Z Modulator Operating at 1.55 μm.
DOI: 10.5220/0005745101620168
In *Proceedings of the 4th International Conference on Photonics, Optics and Laser Technology (PHOTOPTICS 2016)*, pages 164-170
ISBN: 978-989-758-174-8

depletion region might be maximized (Rao et al., 2014).

It is well-known that an increase of the confinement of the optical field inside a guiding structure can be achieved by using photonic crystal waveguides (PhCW) which prohibit the light propagation for specific frequencies within a band-gap, enabling therefore new ways to carry light to and from components of a PEIC (Brimont et al., 2011; Brimont et al. 2009). PhCW, moreover, exhibits near-zero reflection, very low propagating losses through sharp bends (Mekis et al., 1996) and reduced radiation losses (Johnson et al., 1998).

In this paper, in order to take advantage from the strong confinement provided by the PhC structures, the performances of a novel MZI consisting of two coupled p-i-n vertical integrated waveguides surrounded by a two-dimensional (2D) PhC, are performed by a finite-difference time-domain (FDTD)-based software (RSoft).

In such design, we have taken full advantage of the wide tunability of the a-Si:H refractive index, achievable acting on the process parameters during the Plasma Enhanced Chemical Vapour Deposition (PECVD) (Cocorullo et al., 1996), a non-common feature among materials used in photonics.

A schematic representation of the proposed device is shown in Fig.1. The proposed MZI starts with a single mode rib waveguide which splits into two symmetric branches by means of an input splitter. Hence, the two arms become parallels and are surrounded by a proper PhC structure to increase the propagating wave confinement in the waveguide core. One arm acts as an optical phase shifter. To achieve this, a transparent conductive oxide, e.g. sputtered Al-doped ZnO (ZnO/Al) (Della Corte et al., 2011; Rao, 2013), is deposited on the waveguide top to apply a reverse bias to the integrated diode.

At the output, light beams interfere between each other by means a directional coupler.

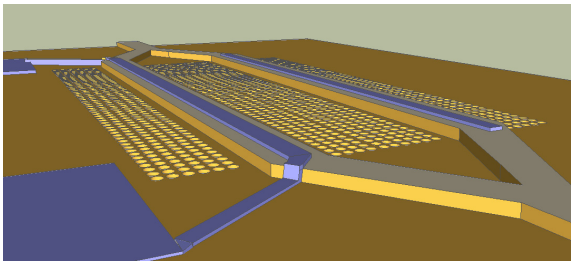

Figure 1: Schematic representation of the proposed device. Dimensions are not in scale.

2 PHOTONIC CRYSTAL WAVEGUIDES DESIGN

For the following analysis, a 2D PhC forming a hexagonal lattice of air rods in an a-Si:H background layer will be considered. It is known that the hexagonal lattice pattern of a PhCW provides the largest band gap among all PhCW geometries allowing to obtain guiding structures which are single mode (SM) and polarization independent (PI) at the wavelength of 1.55 µm (Chen et al., 2009). Moreover, a single-line defect waveguide (SLDW), created by removing a full row of "cylinders", leads to photonic band gaps (PBGs) where the propagating electromagnetic modes are forbidden inside the structure. In order to obtain a PhC geometry with a complete gap (Mekis et al., 1996) and PI (TE and TM), the two materials, in this case air and a-Si:H, should have a high refractive index contrast.

In Fig. 2 we report a generic schematic PhC structure, with hexagonal lattice pattern, in which the circular rods are filled with air. The bulk refractive index was measured in our previous work and used for the realization of a MZI EO modulator (Zelikson et al., 1996; Della Corte 2011 et al.; Rao et al., 2013) ($n_{\text{a-Si:H}}$=3.46).

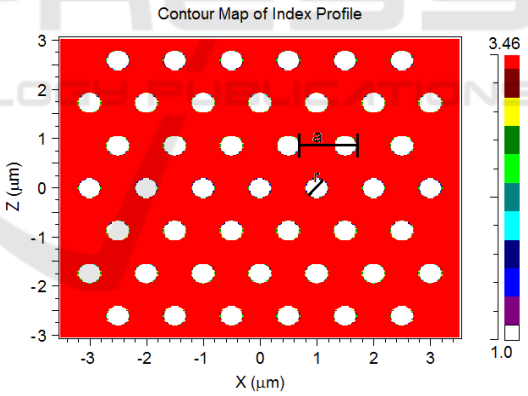

Figure 2: Schematic PhC structure, with hexagonal lattice pattern, and corresponding refractive index colour bar.

In our geometry, the *r* and *a* indicate the rod radius and lattice constant, respectively. The lattice constant was set to 1 µm and subsequently the rod radius varied from 0.1 µm to 0.6 µm in order to find out the optimum value resulting in the widest band-gap for both TE and TM modes. The results of parametric simulation are shown in Fig. 3.

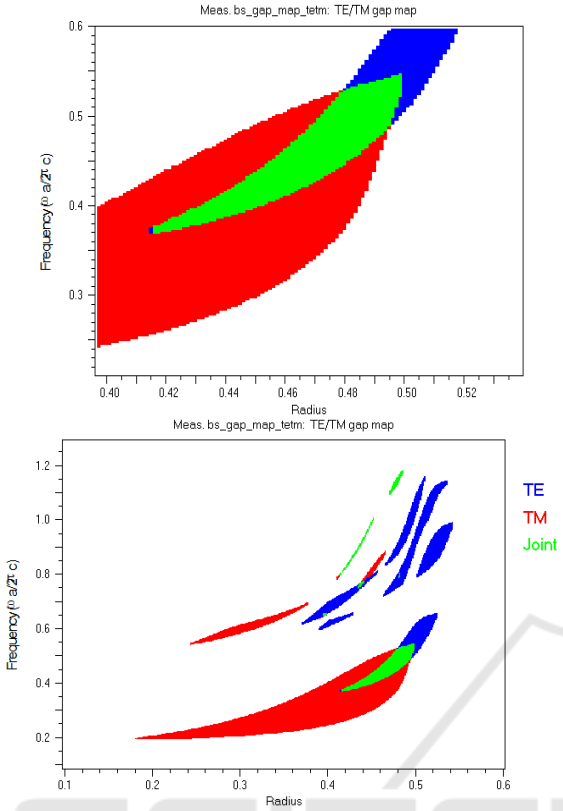

Figure 3: Gap map for the hexagonal lattice PhC.

The photonic bandgap map shown in Fig. 3 introduces red, blue and green marked areas where the TE, TM and both of those modes are not allowed to propagate, respectively. The rod radius values forbidding the propagation of both TE and TM modes (green area) can be seen in detail in the up side of Fig.3.

A rod radius of 0.48 µm provides the widest band gap for our structure presented in Fig.2.

In Fig. 4, the resulting PhC structure is reported together with its refractive index.

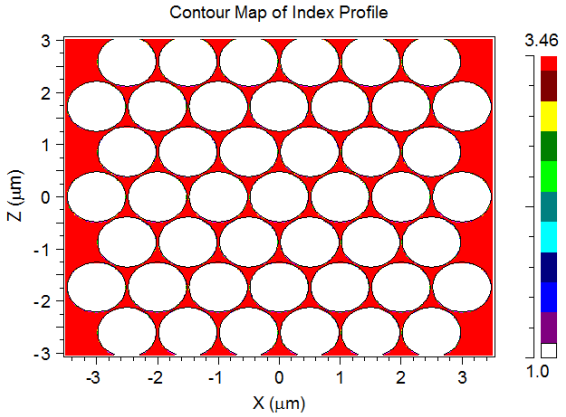

Figure 4: PhC structure, with hexagonal lattice pattern, and corresponding refractive index colour bar.

Subsequently, the PhC structure presented in Fig.4 is simulated through BandSOLVE [17] tool in order to obtain the a/λ ratio and, therefore, the forbidden wavelength range for an optical signal propagating through the PhC. The simulation output is reported in Fig. 5.

Fig. 5 reveals that the simulated PhC structure does not allow the propagation of both TE and TM modes for the hashed area where the a/λ ratio lies between 0.448 to 0.530.

The achieved a/λ ratio values have been also verified through the Fullwave [17] tool by analyzing the stop band range for both TE and TM modes, as reported in Fig. 6, where the red circles highlight the normalized frequency ranges at which both TE (up) and TM (down) modes cannot propagate.

By considering the a/λ ratio varying between 0.448 and 0.53, the forbidden wavelength area is

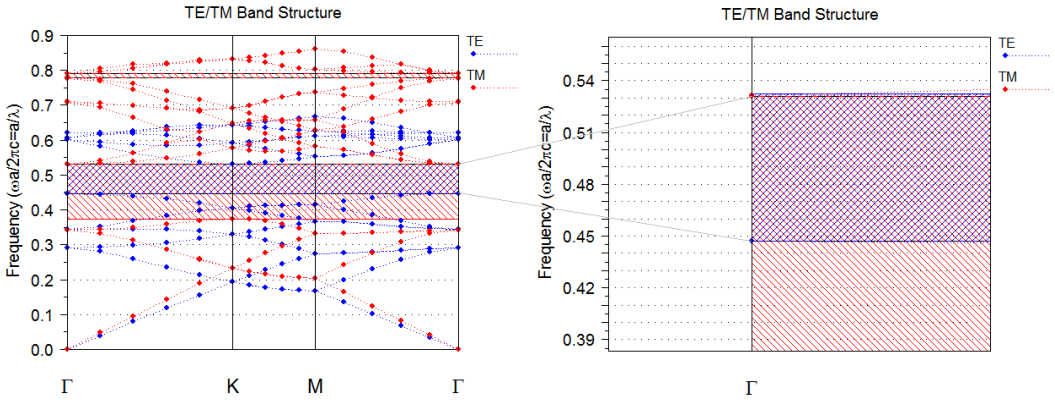

Figure 5: Photonic band structure for both TE and TM modes.

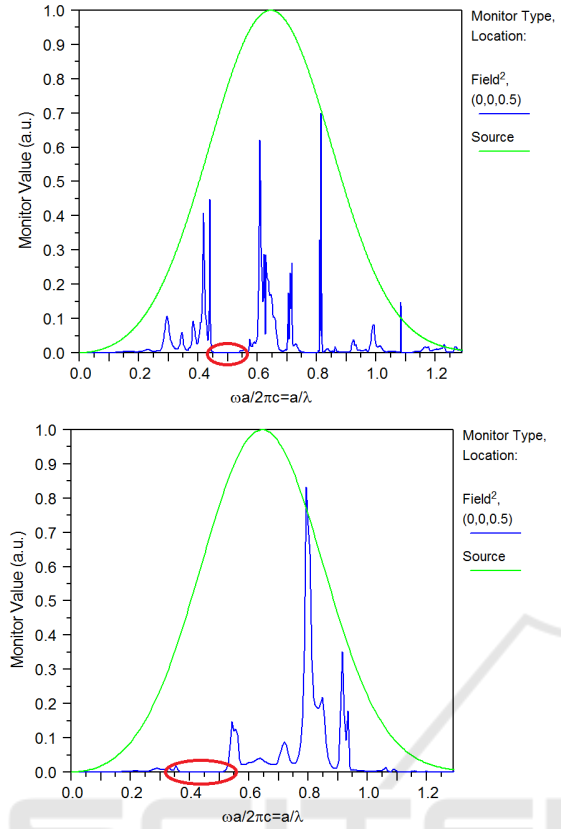

Figure 6: Stop band ranges. The red circles highlight the normalized frequency ranges for TE (up) and TM (down) modes.

calculated by the product of a/λ and r/a (0.48). The resulting forbidden wavelength area for both TE and TM modes covers the wavelengths between 1886 nm and 2232 nm, out of around 1550 nm.

However, for the designed geometry, as shown in Fig. 7, a very thin diaphragm (Delta=40 nm) between two adjacent rods has been obtained, implying consequently a careful and expensive process for the fabrication of the PhC-based active device.

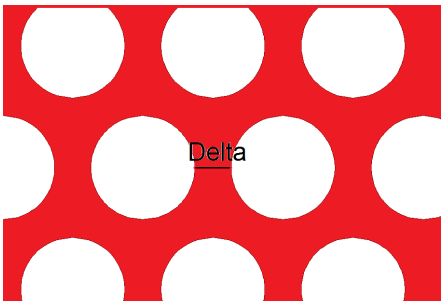

Figure 7: Air rods. "Delta" is the distance between two adjacent rods.

To fully exploit the advantage of the refractive index tunability of a-Si:H by changing the PECVD process parameters (Cocorullo et al., 1996; Rao et al., 2012), parametric simulations have been performed starting from different values of the a-Si:H refractive index in order to investigate if more "relaxed", low cost structures, i.e., less dependent on the fabrication tolerances and technological constraints, could be realized. Moreover, the other goal of the parametric simulations is to evaluate if the resulting structures exhibit polarization dependency.

Polarization dependency and the corresponding forbidden wavelength area of various structures are listed in Table 1.

From Table 1, it can be seen that for an a-Si:H with refractive index n=3.58 (already measured as reported in Ref. (Rao et al., 2010; Rao et al., 2014; Rao et al., 2010; Rao et al., 2010; Rao et al., 2010; Rao et al. 2012; Rao et al., 2012)) the spacing Delta is increased by a factor of five with respect to the value considered in the first simulation. Due to its simple fabrication process and calculated forbidden wavelength area, the PhC structure - radius r=0.4 µm, lattice constant a =1 µm – has been chosen to integrate in the MZI structure. The photonic bands of such structure are shown in Fig.8.

Table 1: Parametric simulation results for different refractive index values.

n	a[µm]	r[µm]	Delta[nm]	TE	TM	λ_{min} [µm]	λ_{max}[µm]
3.46	1	0.48	40	Yes	Yes	1886	2232
3.46	0.76	0.36	40	Yes	Yes	1496	1715
3.46	0.59	0.25	90	Yes	Yes	1512	1573
3.46	0.47	0.18	110	No	Yes	1245	1993
3.52	1	0.39	220	Yes	No	1511	1586
3.58	1	0.4	200	Yes	Yes	1531	1565

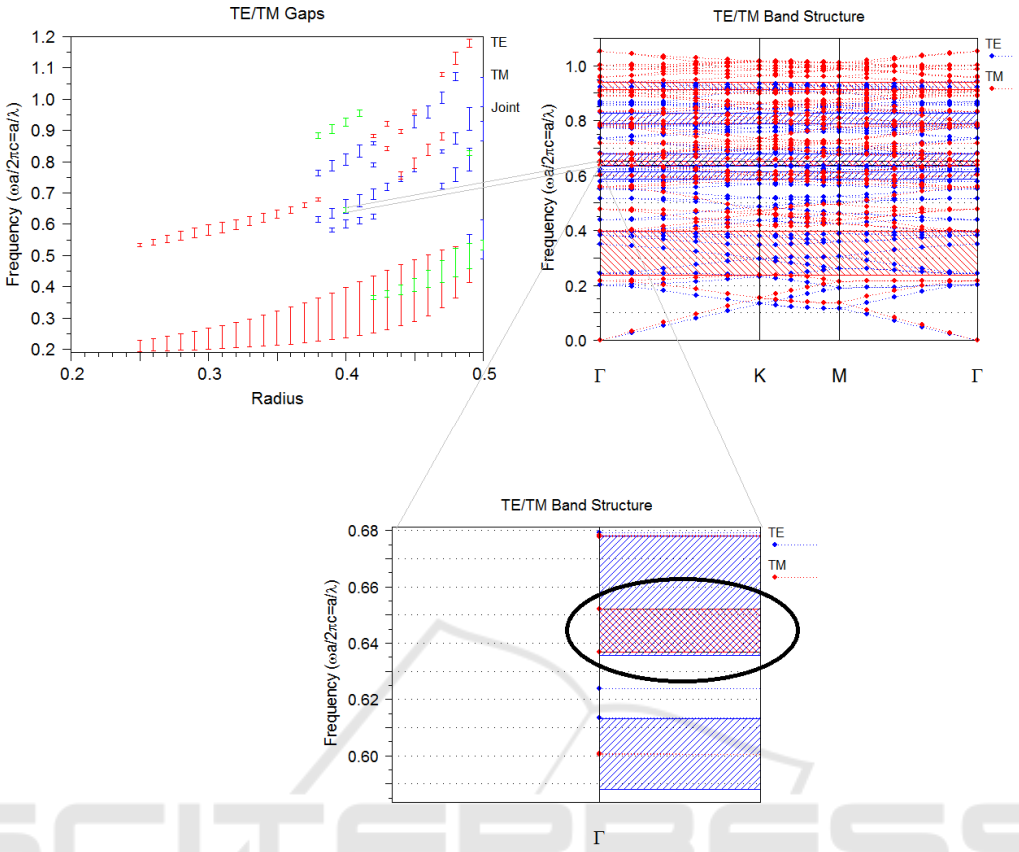

Figure 8: Photonic band structure for both TE and TM modes.

3 PHC MZI DESIGN AND SIMULATION RESULTS

The designed PhCW has been integrated inside a MZI in order to evaluate the phase shift, ΔΦ, induced in the active arm by monitoring the output intensity, which is given by (Chen et al., 2009):

$$I_{out} = \frac{I_{in} + I_{in} \cdot \cos(\Delta\phi)}{2}$$

where I_{in} and I_{out} are the MZI input and output light beam intensities, respectively.

One can further derive the effective index change Δneff of the waveguide mode using the equation:

$$\Delta\phi = \frac{2\pi}{\lambda} \Delta n_{eff} L$$

where L is the active length of the phase shifter, and λ is the wavelength in the free space. A schematic of the PhCW structure, for Δn_{eff} estimation, is depicted in Fig. 9.

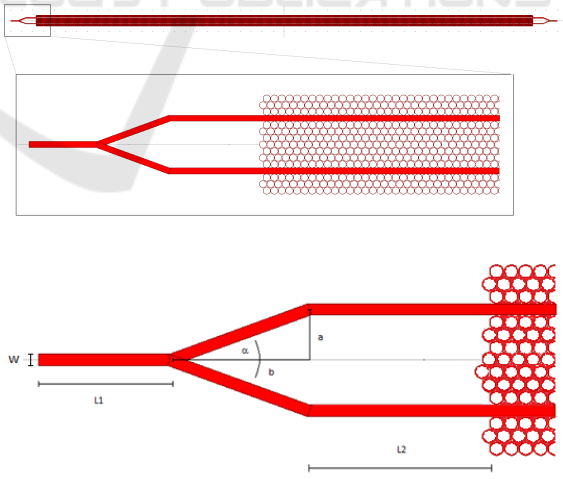

Figure 9: Schematic structure of the PhCW integrated inside a MZI.

Parametric simulations were performed to calculate the optimum values of the overall geometric parameters reported in Fig. 9. In particular the intersecting angle α for the input and output MZI

splitter has been determined in order to achieve a trade-off between the need for a compact device and low insertion losses. The device geometries have been optimized in order to achieve birefringence-free, SM propagation and acceptable coupling losses to standard SM fibers with cleaved termination.

Simulation results are well summarized in the following table:

Table 2: Parametric simulation results. The reported device geometries have been optimized in order to achieve birefringence-free, SM propagation and low coupling losses.

W [µm]	L1 [µm]	a [µm]	b [µm]	α [°]	L2 [µm]
1	100	4	573	0.8	100

Moreover, the impact of the refractive index change induced in only one arm of the MZI (surrounded by the PhC structure) was investigated for different lengths. We designed, in fact, MZIs with arm lengths of L=0.5 mm, 1 mm and 1.5 mm.

As already mentioned, the refractive index change can be induced through the free carrier dispersion effect and therefore it is controlled by the carrier concentration profile. By reverse biasing the device, we can induce a modulation of the space charge volume that, in turn, modifies the refractive index profile of the waveguide and therefore the optical phase of the 1.55 µm wavelength light passing through it (Zelikson, 1992).

Fig. 10 (a) shows the normalized optical signal at the MZI output as a function of the effective refractive index change (Δn_{eff}) induced in MZI arms of different lengths, while Fig. 10 (b) reports the effective refractive index variation required to induce a phase shift of $\Delta\Phi=\pi$, between the two optical beams, for arms of different lengths.

By using the same $\Delta n/\Delta V$ calculated and experimentally measured for the a-Si:H MZI reported in our previous work (Zelikson et al., 1992), characterized by an arm length of 13 mm, we can conclude that with the newly designed PhC-based device we can obtain a full π-shift in a 1.5 mm-long arm by applying the same driving signal (~30V), with a consequent reduction of the $V_\pi \times L$ FoM from 40 V×cm to 4.5 V×cm.

It should be finally considered that a thinning of the waveguide core can allow a further reduction of the driving signal amplitude necessary for a π-shift, as the bias to drive in full depletion a p-i-n device scales with a square law of the thickness of the intrinsic region, as reported in Fig. 11.

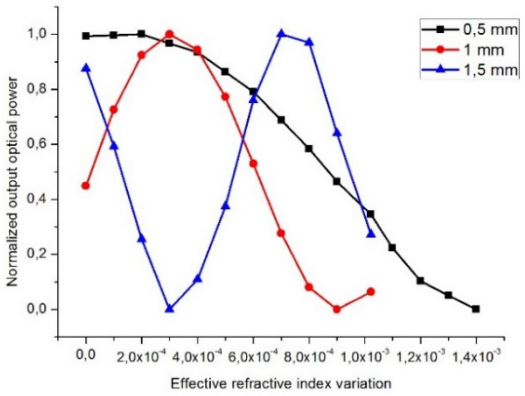

(a)

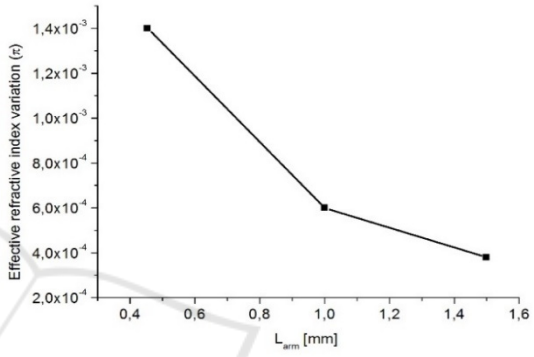

(b)

Figure 10: (a) Normalized transmitted MZI optical power vs. effective refractive index variation (Δneff) and (b) effective refractive index variation (Δneff(π)) for inducing a phase shift of $\Delta\Phi=\pi$ for the three considered MZI arm-lengths.

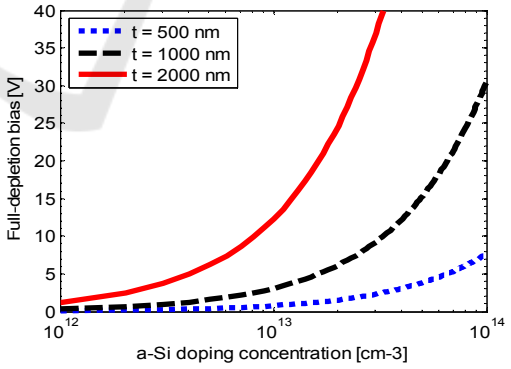

Figure 11: Calculated full depletion bias of a p-i-n waveguide as a function the i-layer doping. The three curves refer to different i-layer thicknesses (Della Corte et al., 2011).

The proposed device, therefore, can even work with lower driving voltage allowing a FoM as low as of that observed in performing electro-optical modulators in silicon (Reed et al., 2010).

4 CONCLUSIONS

In this work, numerical simulations of a PhC MZ modulator based on a-Si:H and working at 1.55 μm, are reported. Our FDTD numerical simulations show that taking advantage from both the tunability property of the a-Si:H physical parameters and the strong optical beam confinement within a PhCW, a more efficient phase shifting can be obtained in the interferometric structure. Our results show that the FoM is enhanced of an order of magnitude with respect to our previously realized active device based on the electrically induced free carrier dispersion effect. In fact, by reverse biasing the vertical p-i-n diode integrated into the PhCWs, 1.5 mm-long, we achieved a reduction of the $V_{\pi}\times L$ voltage-length from 40 to 4.5 V×cm and we predicted as much reduction for sub-micron waveguide core thickness. Moreover, the corresponding PhC fabrication process does not require sophisticated technological facilities leading therefore to a truly low cost technology.

REFERENCES

Vlasov, Y. et al., 2005. Active control of slow light on a chip with photonic crystal waveguides. Nature, 438(7064), pp.65–69.

Reed, G. T. et al., 2010. Silicon optical modulators. Nature Photonics 4 (8), pp.518 – 526.

Della Corte, F.G. & Rao, S., 2013. Use of amorphous silicon for active photonic devices. IEEE Transactions on Electron Devices, 60(5), pp.1495–1505.

Rao, S. et al., 2012. A 2.5 ns switching time Mach-Zehnder modulator in as-deposited a-Si:H. Optics Express, 20(9), p.9351.

Zelikson, M. et al., 1992. Enhanced electro-optic effect in amorphous hydrogenated silicon based waveguides. Applied Physics Letters 61(14), pp.1664–6.

Zelikson, M. et al., 1996. Direct determination of the quadratic electro-optic coefficient in an α-Si:H based waveguide. J. Non-Cryst. Solids 198–200, pp.107–10.

Della Corte, F.G. et al. 2008. Electro-optically induced absorption in a-Si:H/a-SiCN waveguiding multistacks. Optics Express, 16(10), pp.7540-7550.

Rao, S. et al., 2010. Electrooptical Modulating Device Based on a CMOS-Compatible a-Si:H/a- SiCN Multistack Waveguide. IEEE Journal of Selected Topics in Quantum Electronics, 16(1), pp.173–178.

Della, F.G. et al., Hydrogenated amorphous silicon multi-SOI waveguide modulator with low voltage – length product.

Rao, S. et al., 2014. Progress towards a high-performing a-Si:H-based electro-optic modulator. Journal of Optics, 16(5), p.055501.

Della Corte, F.G. et al., 2011. Electro-optical modulation at 1550 nm in an as-deposited hydrogenated amorphous silicon p-i-n waveguiding device. Optics express, 19(4), pp.2941–2951.

Rao, S. & Della Corte, F.G., 2014. Numerical analysis of electro-optical modulators based on the amorphous silicon technology. Journal of Lightwave Technology, 32(13), pp.2399–2407.

Brimont, A. et al., 2011. High speed silicon electro-optical modulators enhanced via slow light propagation. , 19(21), pp.21986–21991.

Brimont, A. et al., 2009. Strong electro-optical modulation enhancement in a slow wave corrugated waveguide. Optics express, 17(11), pp.9204–9211.

Mekis, A. et al., 1996. High Transmission through Sharp Bends in Photonic Crystal Waveguides. Physical Review Letters, 77(18), pp.3787–3790.

Johnson, S.G. et al., 1998. Elimination of cross talk in waveguide intersections. Opt. Lett. 23, pp.1855-1857.

RSoft Photonics CAD Layout User Guide, Rsoft Design Group, Inc. Physical Layer Division, 200 Executive Blvd. Ossining, NY 10562.

Cocorullo, G. et al., 1996. Amorphous silicon waveguides and light modulators for integrated photonics realised by low-temperature plasma enhanced chemical vapour deposition. Optics Letters, 21(24), pp.2002-2004.

Rao, S., 2013. Hydrogenated amorphous silicon phase-change device based on a p–i–p waveguiding configuration. Optics & Laser Technology 53, pp.17-21.

Chen, X. et al., 2009. Electrooptically-active slow-light-enhanced silicon slot photonic crystal waveguides. IEEE Journal on Selected Topics in Quantum Electronics, 15(5), pp.1506–1508.

Rao, S. et al., 2013. Electro-optical effect in hydrogenated amorphous silicon-based waveguide-integrated p-i-p and p-i-n configurations. Optical Engineering, 52(8), p.087110.

Rao, S. & Della Corte, F.G., 2012. 1.55 □m Silicon-Based Reflection-Type Waveguide-Integrated Thermo-Optic 2×2 Switch. Optik - International Journal for Light and Electron Optics, 123(5), pp.467–469.

Rao, S. et al., 2010. Electro-optically induced absorption in α-Si:H/α-SiCN waveguiding multistacks. Journal of the European Optical Society, 5, pp.10002.

Rao, S., &Della Corte, F.G., 2010. Electro-optical modulating multistack device based on the CMOS-compatible technology of amorphous silicon", Journal of the European Optical Society, 5, pp.10040.

Rao, S. et al., 2010. Low-loss amorphous silicon waveguides grown by PECVD on indium tin oxide. Journal of the European Optical Society, 5, pp.10039.

Rao, S., Della Corte, F.G. & Summonte, C., 2012. Amorphous silicon waveguides grown by PECVD on an Indium Tin Oxide buried contact. Optics Communications, 285(13-14), pp.3088–3092.

Rao, S. et al., 2012. All-optical modulation in a CMOS-compatible amorphous silicon-based device. Journal of the European Optical Society, 7, pp.12023.